IEEE Access
Multidisciplinary | Rapid Review | Open Access Journal

Received January 31, 2021, accepted February 16, 2021, date of publication February 22, 2021, date of current version March 3, 2021.

Digital Object Identifier 10.1109/ACCESS.2021.3060348

Integrating Pre-Earthquake Signatures From Different Precursor Tools

ESSAM GHAMRY[1,2], EMAD K. MOHAMED[1], MOHAMED S. ABDALZAHER[1], (Member, IEEE), MOHAMED ELWEKEIL[3], DEDALO MARCHETTI[4,5], ANGELO DE SANTIS[4,6], MOSTAFA HEGY[1], AKIMASA YOSHIKAWA[2], AND ADEL FATHY[7]

[1]National Research Institute of Astronomy and Geophysics, Cairo 11421, Egypt
[2]International Center for Space Weather Science and Education, Kyushu University, Fukuoka 819-0395, Japan
[3]Department of Electronics and Electrical Communications Engineering, Faculty of Electronic Engineering, Menoufia University, Menouf 32952, Egypt
[4]INGV Istituto Nazionale di Geofisica e Vulcanologia, 00143 Rome, Italy
[5]The College of Instrumentation and Electrical Engineering, Jilin University, Changchun 130061, China
[6]Earth Sciences Department, Rome La Sapienza University, 00185 Rome, Italy
[7]Physics Department, Faculty of Science, Fayoum University, Fayoum 63514, Egypt

Corresponding authors: Essam Ghamry (essamgh@nriag.sci.eg), Mohamed S. Abdalzaher (msabdalzaher@nriag.sci.eg), and Mohamed Elwekeil (mohamed.elwekeil@el-eng.menofia.edu.eg)

This work was supported by JSPS KAKENHI under Grant JP20H01961 and Grant JP15H05815.

ABSTRACT Potential earthquake precursors include, among others, electromagnetic fields, gas emissions, Land Surface Temperature (LST), Sea Surface Temperature (SST), and Surface Air Temperature (SAT) anomalies. These observables have been individually studied, before earthquakes, by many researchers. The ionospheric studies concerning earthquakes (EQs) using magnetic data from Low Earth Orbit (LEO) satellites are increasingly being used to detect ionospheric anomalies before large EQs. Also, LST, SST, and SAT values retrieved from Moderate Resolution Imaging Spectroradiometer (MODIS) Terra and Aqua satellites and Modern-Era Retrospective analysis for Research and Applications Version 2 (MERRA-2) are considered as physical precursors before EQs. In this work, we jointly analyze magnetic, MODIS, and MERRA-2 data in space and time around the epicenters before the selected EQs in Mexico, Japan, Chile, and Indonesia. Our analyses present interesting findings where anomalies in temperature and magnetic field, preceding the considered EQs, are confirmed through different methods. Particularly, we utilize the Fast Fourier Transform (FFT) and the Discrete Cosine Transform (DCT) for analyzing magnetic data over the designated EQs regions. We use the magnetic data acquired by Swarm satellites in the top side ionosphere along with MODIS and MERRA-2. Five case studies are described to prove the effectiveness of our analyses. Precursory anomalies were observed using these methods in different anomalous days from the considered four regions of interest around the epicenter. It is concluded that these methods could be effective and reliable in detecting anomalies preceding the upcoming EQs.

INDEX TERMS Swarm satellite mission, earthquake precursors, magnetic anomaly, MODIS and MERRA-2 data, Fast Fourier Transform (FFT), Discrete Cosine Transform (DCT).

I. INTRODUCTION

Large earthquakes (EQs) stimulate co-seismic ionospheric disturbances, known as Seismo-Travelling Ionospheric Disturbances (STIDs). The STIDs propagate from the epicenter of the EQ into the ionosphere like a circular wave. These STIDs can be detected by instrumentation on the ground and in space [1], [2]. Some researchers explored the possibility that such phenomena could happen even before the seismic event and with other paths toward the ionosphere and in general all of these phenomena are called the Lithosphere Atmosphere Ionosphere Coupling (LAIC) effects, described by analogous model. The history of the LAIC model dates back to 1994 when [3] reported several aspects such as natural radioactivity, aerosols, and atmospheric electricity which is an alternative way to explain the seismo-ionospheric variations. Then, [4], [5] gave the first version of the model. After that, many proposals were presented to explain the effect of LAIC in the ionosphere [6]–[12]. The authors in [5] stated that at the EQs, volcanoes, and active tectonic faults

The associate editor coordinating the review of this manuscript and approving it for publication was Wei Wang.

could make an essential contribution to the global electric circuit and the ionosphere variability. [13] demonstrated the synergy between the evolution of thermal and electromagnetic anomalies in the Earth's atmosphere, ionosphere, and magnetosphere. In the last centuries, non-seismic strange phenomena have been observed on occasion of strong EQs. These non-seismic phenomena comprise magnetic field variations, electromagnetic emissions in the range of ULF/ELF frequencies (1 mHz to 10 Hz), ground radon emissions, water condensation in the atmosphere, and gravity waves rising to the ionosphere [7], [8]. Several researchers made an integrated and multidisciplinary approach, ionospheric and surface thermal data attempting to identify possible precursor signals. Also, many researchers have studied the earthquake precursors [14]–[16] specially LST anomaly as earthquake precursor which studied by [17]–[22]. The increase in land surface temperatures (LST) during seismic activity are related to stresses and subsurface degassing [23], [24]. During the plate movement, the temperature increases with the increase in pressure and thus the stress in such region may cause LST anomalies. Further, these stresses may cause subsurface degassing, and these gases produce local greenhouse effect and increase the temperature of the region. This theory is proposed based on the charge generation in rocks before earthquakes [10], [25]–[30].

The ionosphere is a region extending from about 50 to 1000 km above the earth's surface and plays a crucial role in the radio-wave propagation [31], [32]. In the last few decades, in the upper ionosphere, Low Earth Orbit (LEO) satellites have given some unique opportunities, and a lot of information to investigate the effect of the ionosphere on waves propagation. For example, the three Swarm spacecraft (Swarm-Alpha, Swarm-Charlie, and Swarm-Bravo) were launched by European Space Agency on 22 November 2013 into a quasi-polar LEO with an initial altitude of about 510 km [33]. These spacecraft were used to search for any abnormal anomalies which could be related to seismic activities. The authors in [34] provide evidence that precursory signals can be observed before the large EQs by days, weeks, or months. Recently, [35]–[37] made some analyses of particular case studies, and found clear magnetic variations in the ionosphere associated with large EQs using data from Swarm satellites.

Since the advent of data availability era is started using satellites, the visual and manual inspection of such time series makes the analysis task complex. Spectral analysis techniques such as Fast Fourier Transform (FFT), Discrete Fourier Transform (DFT), wavelet, and Maximal Overlap Discrete Wavelet Transform (MODWT) contribute to quick, reliable, and efficient detection of anomalous patterns [38]–[43]. Besides, the Moderate Resolution Imaging Spectroradiometer (MODIS) has been considered in [44] to study the temperature anomaly preceding 2016 Ecuador Mw = 7.8 EQ togheter with the elaboration of the Swarm magnetic and plasma data.

In this paper, FFT and Discrete Cosine Transform (DCT) transforms are used to identify possible precursory variations in the earth's magnetic field due to seismic events. Also, we used the collection V6 of MODIS Land Surface Temperature (LST) product (MOD11A1) and Sea surface temperature (SST) products of Moderate Resolution Imaging Spectroradiometer (MODIS, Level 3) with a spatial resolution of 4 km were derived from the MODIS sensors onboard Terra and Aqua platforms. (LST) data has been validated at the first stage with in situ measurements in more than 50 clear-sky cases in the temperature range from 10° to 58° [45], [46]. Detailed validation of the C6 MODIS LST product is given by [47]. Moreover, Modern-Era Retrospective analysis for Research and Applications, Version 2 (MERRA-2) Surface Air Temperature (SAT) is used.

We consider five case studies, the first three of them reported by [35], [36] and the fourth one reported by [48]. It should be noted that the works presented in [35], [36] considered only the anomalies in the space magnetic fields. Unlike [35], [36], we incorporate anomalies in Swarm magnetic field, LST and SAT before five large EQs (Southern Mexico 8^{th} September 2017 of M8.2, Japan 15^{th} April 2016 of M7.0, Chile 1^{st} April 2014 of M8.2, Indonesia 2^{nd} March 2016 of M7.8, and Indonesia 28^{th} September 2018 of M7.5). The main goal of the paper is to jointly analyze anomalies from different sources preceding large EQs. Specifically, we analyze the Swarm satellite magnetic data using Analysis of Magnetic SWarm (AMSW) algorithm and two spectral analysis methods (FFT and DCT). Furthermore, we utilize the LST,SST and SAT data to extract the corresponding anomalies. Detecting thermal anomalies and evaluating LST, SST and AST components carried out by combining thermal remote sensing time series data. To the best of our knowledge, this work is the first to jointly consider AMSW, DCT, FFT, MODIS and MERRA-2 analyses for detecting anomalous events that occur before large EQs. Furthermore, it is the first work that considers DCT transform for analyzing the magnetic field anomalies that precede large EQs.

The paper is organized as follows: in section II, we describe the data sets along with EQ and satellite track selection criteria; section III presents the methodologies employed in our analyses; section IV presents our observations and results; then, section V compare the observations; and section VI summarize our conclusions.

II. DATA SETS

A. SWARM DATA

In this paper, we use data from Swarm mission. The three Swarm spacecraft (Swarm-Alpha, Swarm-Charlie, and Swarm-Bravo) were launched on 22 November 2013 into a quasi-polar LEO with an initial altitude of about 510 km [33]. Since April 2014, Swarm-Alpha (SW-A) and Swarm-Charlie (SW-C) have been spinning on nearly identical orbits at

460 km altitude with latitudinal and longitudinal separations less than 1.5°, and an inclination of 87.4°. Meanwhile, Swarm-Bravo (SW-B) has been operated at a slightly higher altitude of 510 km with an inclination of 87.8°. In this study, we use the 1 Hz magnetic field data from Vector Field Magnetometer (VFM) onboard Swarm. The original data were provided in the North-East-Center (NEC) local coordinate frame (magnetic product: MAGX_LR_1B). The Swarm satellites are equipped by sophisticated magnetometers to measure, in an accurate way, accelerometers, intensities of the magnetic and the electric fields, etc.

B. MODIS LST DATA

MODIS sensor was launched in 1999 and 2002 on board the Terra and Aqua Satellites, respectively. It can observe ocean, atmosphere, land, and ice for many scientific fields. MODIS Terra LST data product MOD11A1 have been used to find the correlation between the thermal anomalies and seismic activity. The MOD11A1 V6 product supports LST and Emissivity (LST&E) with 1 km spatial resolution in a grid of 1200 by 1200 km. The LST&E values are retrieved by the generalized split-window algorithm [49]. In this study, the MODIS sensor was considered instead of Landsat or ASTER because MODIS data have high temporal resolution in comparison with Landsat and ASTER data. This is because the earthquakes have an impact on a large scale and daily data are important to analyze the spatio-temporal anomalies.

C. MODIS SST DATA

The Sea surface temperature (SST) daily mean global data retrieved from the Moderate Resolution Imaging Spectro-radiometer (MODIS, level 3) with a spatial resolution of 4 km were used to fill the gap of LST data and support the derived results. The MODIS SST products were extracted from the Ocean Color [50].

D. MERRA-2 SAT DATA

Modern-Era Retrospective analysis for Research and Applications, Version 2 (MERRA-2) is a climatological data obtained by re-analysis of atmospheric data retrieved originally by meteorological stations, satellite data, atmospheric sounding and more [51]. MERRA-2 is provided by NASA-NOAA with data started from 1980 and continuously updated. The data are provided on a regular grid with a spatial resolution is 0.625 in longitude and 0.500 degree in latitude at each UT o'clock time.

E. EARTHQUAKE AND SATELLITE TRACK SELECTION

The main criteria of an EQ selection are: (1) Its occurrence in a geomagnetic quiet time to exclude the external sources of ionospheric disturbances; (2) The satellite should pass above the epicentral region inside the Dobrovolsky's area which is considered a sufficient approximation of the EQ preparation region, where researchers usually use it [35], [36], [52], [53]; (3) The shallow EQs (depth $\leq$ 50 km) with M5.5+ are taken into account to exclude any possible coseismic effect due to smaller event with respect to the mainshock. Note that the Dobrovolsky's area (RDb) is a circular region that depends on the magnitude of the EQ where RDb (km) $= 10^{0.43Mw}$ [54].

III. METHODOLOGIES

In our analysis, we consider several methodologies for detecting pre-EQ anomalies. First, we employ AMSW analysis, FFT transform, and DCT transform to analyse the space magnetic field anomalies before large EQs. Furthermore, we have used MODIS LST and MERRA-2 data to detect temperature anomalies that could occur before large EQs.

A. AMSW ALGORITHM

In this part, we will describe the AMSW algorithm, which is similar to MAgnetic Swarm anomaly detection by Spline analysis (MASS) algorithm [35]. Unlike the MASS algorithm, the AMSW algorithm uses the CHAOS-6 model [55]. AMSW algorithm steps are as follows: we first confirm that the utilized data corresponds to the quiet times in the day. Then, we extract data from the original 1 Hz time resolution Common Data Format (CDF) vector file. After that, we convert the geographic latitude to geomagnetic latitude and compute the corresponding local time, LT.

The VFM data represents the total magnetic field. Accordingly, we have used the CHAOS-6 model [55] of Earth's geomagnetic field, which has been developed using more than 6.5 years of high-precision geomagnetic measurements from the three satellites, to retrieve the external ionospheric component. The first time derivative, with knot points every 20 s, is applied to the residual data for displaying more information from the data. We apply these analyses to the three orthogonal components of the geomagnetic field, B_x, B_y, and B_z, that point toward North, East, and Earth center, respectively, and then, the residual is investigated. A track is considered anomalous when the Y component residuals of pick amplitude overpass 0.3 nT/s with a persistence of 10s [56], [57] and there are more than 5 points that are outliers, i.e. outside 3 standard deviations with respect to the distribution of the residuals of the track (calculated only by subtracting the CHAOS-6 model and first time derivative).

B. FFT TRANSFORM

The frequency domain is utilized to show the signal properties and components within every frequency band over a range of frequencies. Moreover, this domain contains information about the signal phase shift that can be used to retrieve the original signal in the time-domain. Frequency domain extensively depicts the signal energy distribution [58]. Several transformations have been developed to represent the signal in the frequency domain such as FFT and DCT. FFT is among the powerful computational methodologies to study signals in the frequency domain, which rapidly illustrates the signal components. It is an effective technique for computing the DFT of a time series [59]. FFT relies on the iterative calculations of the DFT coefficients that result in notable

economical computation time. FFT is given by

$$\omega(k) = \sum_{n=0}^{N-1} f(n) e^{\frac{-2j\pi kn}{N}}, \quad k = \{0, 1, \cdots, N-1\}, \quad (1)$$

where $\omega(k)$, is the k^{th} coefficient of the FFT and $f(n)$ denotes the n^{th} sample of the time series which consists of N samples and $j = \sqrt{-1}$. The $f(n)$'s can be complex numbers and the $\omega(k)$'s are almost always complex. We apply the FFT on the derivatives of the residual of the three orthogonal magnetic field components, with respect to CHAOS-6, in periods that precede an EQ to get insights about their frequency domain components. In other words, $f(n) = \frac{d\gamma(n)}{dt}$ can be calculated by

$$\frac{d\gamma(n)}{dt} = \frac{\gamma(n) - \gamma(n-1)}{\Delta t}, \quad (2)$$

where $t = n\Delta t$ with Δt is the sampling interval. In this context, $\gamma(n)$ in (2) can be substituted by, B_x, B_y, and B_z for the three magnetic field components.

C. DCT TRANSFORM

The DCT was firstly introduced to be utilized for various signal processing applications such as pattern recognition, filtering, and data compression [60]. DCT is able to find a representation for signals, especially low-frequency signals, with only a few coefficients. The DCT transform of a time-domain data sequence, i.e., sampled signal, $f(n), n \in \{0, 1, 2, \cdots, N-1\}$ is given by

$$\varphi(k) = \sum_{n=0}^{N-1} f(n) cos(\frac{(2n+1)\pi k}{2N}), \quad k = \{0, , 1, \cdots, N-1\}, \quad (3)$$

where $\varphi(k)$ is the k^{th} DCT coefficient. The motivation to use DCT in analyzing the magnetic events, which precedes earthquakes. Specifically, we propose to analyze the three orthogonal magnetic field components B_x, B_y, and B_z by finding the DCT coefficients that can represent 99.9% of the event energy. Let the sequence $\mathbf{v} = (\varphi(1), \varphi(2), \cdots, \varphi(N-1))$. First, we calculate the time series, $\mathbf{p} = |\mathbf{v}|$, which contains the absolute values of the sequence $\mathbf{v}$ entries. Then, we sort this sequence $\mathbf{p}$ in a descending order where we get the sorted sequence $\mathbf{s} = (b_1, b_2, \ldots, b_{N-1})$, where $b_i > b_{i+1}, \forall i \in \{1, 2, \ldots, N-2\}$. Then, we define $\mathbf{s}_d = (b_1, b_2, .., b_d)$ which contains the first d components of $\mathbf{s}$, where d is the smallest number that satisfies

$$\frac{\|\mathbf{s}_d\|}{\|\mathbf{s}\|} \geq 0.999 \quad (4)$$

D. MODIS LST AND SST APPROACHES

In the MODIS data, the generalized split-window algorithm of [49] is commonly applied to retrieve LST from clear-sky pixels. The fundamental theoretical description for the LST algorithm is given by

$$L(\lambda, T_s) = \epsilon(\lambda)\beta(\lambda, T_s), \quad (5)$$

where the emitted spectral radiance, L, at wavelength λ from a surface at thermodynamic temperature T_s is given by multiplying the Planck function, $\beta(\lambda, T_s)$, by spectral emissivity, $\epsilon(\lambda)$.

The LST values retrieved from MOD11A1 product V6 using the following steps: 1) getting the available product data for the region of interest, 2) extracting data in (hdf) file format, 3) finally, the LST values were extracted in Kelvin for all images. The pathfinder SST algorithm was derived from the split-window non-linear SST (NLSST) formulation [61]. The MODIS LST and SST products are used to investigate the changes in the local atmospheric and oceanographic conditions associated with the selected earthquakes. In order to determine the anomaly of temperature, standard deviation (σ) of mean values were determined and $\pm 2\sigma$ (95% confidence level) interval was utilized as anomaly indicator. In this measure, $mean - 2\sigma$ and $mean + 2\sigma$ are considered as LB and UB, respectively, as given by the following Equations:

$$UB = meanvalue + 2\sigma, \quad (6)$$

$$UB = meanvalue - 2\sigma \quad (7)$$

E. MERRA-2 SAT APPROACH

The Surface Air Temperature data of MERRA-2 SAT have been retrieved for the same day investigated with the magnetic data. The area has been chosen to include the magnetic anomaly, so a comparison of the two observables to understand if a ground warming is present during the magnetic anomaly. These data are an integration of the MODIS data and we expect similar results. The main difference is that MODIS data are direct observation from Earth Observation satellite, while MERRA-2 comes from model fit over observation. The model have the advantage to work even in particular atmospheric conditions, such as with cloud by the integration of the data with several sources. A background has been computed pixel-by-pixel by the values of the previous 10 years in the same UT time-day-month (for example: 21-3-2006, 21-3-2007, …21-3-2015 to compute the background of the 21-3-2016). Two maps are produced: the left one represents the value of the Surface Air temperature of the day of the magnetic anomaly minus the background and the right one shows the standard deviation of the background. The standard deviation is represented to check whether the eventual deviation in the left map is significant or typical for that region in those season.

IV. OBSERVATIONS AND RESULTS

This section presents the most interesting findings of our analysis. Here, we study five pre-EQ anomalies. Using the implemented methods, the analyzed EQs show reliable results, in which the anomalous events in space magnetic field, LST and SAT can be utilized as EQ precursors. Furthermore, we show the results obtained from AMSW analysis, FFT transform, and DCT transform.

A. FIRST CASE STUDY (08 SEPTEMBER 2017 Mw = 8.2 PACIFIC COAST OF SOUTHERN MEXICO EQ)

Figure 1 shows the results for an anomalous event detected by the SW-C satellite on 21^{st} June 2017, about 80 days before an Mw = 8.2 EQ that struck off the pacific coast of Southern Mexico on 8^{th} September 2017 with epicenter at 15.022°N 93.899°W. This EQ was the most powerful to hit the area in 100 years and, led to fatal consequences including dozens of deaths and severe damage in thousands of homes. Specifically, figures 1.a, 1.b, and 1.c depict the AMSW algorithm results for the three magnetic field components B_x, B_y, and B_z, respectively where mean UTC = 11:34, mean LT = 05:18, Dst = -5nT. Figure 1.d shows the location map of the EQ, where the red line is the Swarm C track and the green circle shows the Dobrovolsky's area. Figure 2 shows the

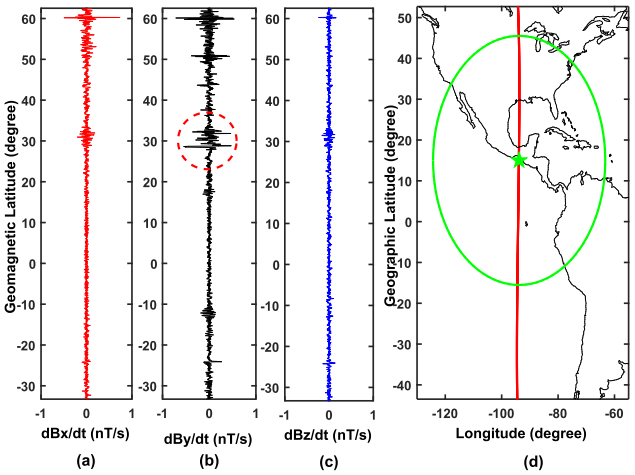

FIGURE 1. Anomalous event detected by AMSW algorithm on 21^{st} June 2017 at SW-C, i.e., 80 days before the 8^{th} September 2017 Mw = 8.2 Pacific coast of Southern Mexico EQ. Green oval around the epicenter is the Dobrovolsky's area.

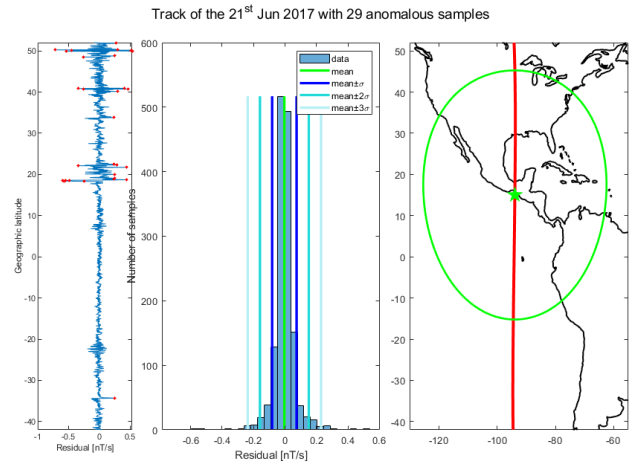

FIGURE 2. Residual of Y component of magnetic field of Swarm Charlie on 21^{st} June 2017 around M8.2 Mexico earthquake. A geographical map with red projection of the track and the histogram of the residuals are represented.

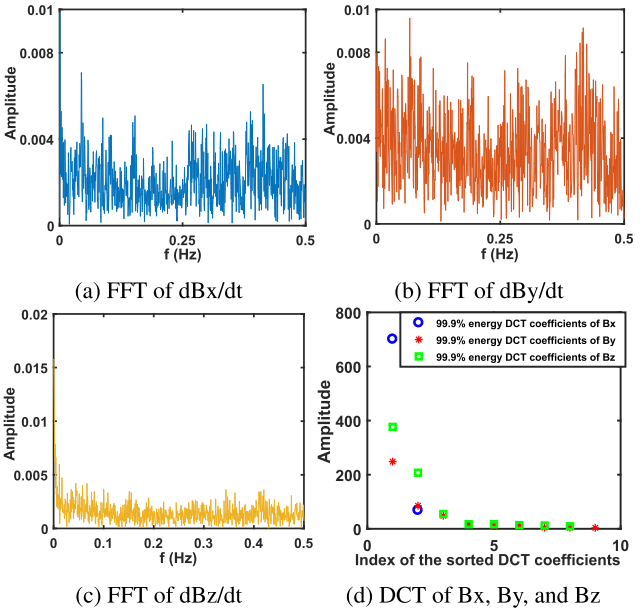

FIGURE 3. Spectral analysis output confirms the anomalous event detected by AMSW algorithm in figure 1.

residual of Y-component of magnetic field of SW-C on 21^{st} June 2017 around M8.2 Mexico earthquake. A geographical map with red projection of the track and the histogram of the residual are represented.

Besides, the amplitude spectrum for $\frac{dB_x}{dt}$, $\frac{dB_y}{dt}$, and $\frac{dB_z}{dt}$, are shown in figures 3a, 3b, and 3c, respectively. Furthermore, figure 3d depicts the DCT coefficients that contains 99.9% percent of the three magnetic field components. It is noteworthy that the B_x, B_y, and B_z components can be represented by only 2, 9, and 8 DCT coefficients, respectively. This is because the anomalous space magnetic events are of ULF. We employ this fact to identify this kind of events using DCT.

Furthermore, the MODIS LST images were acquired and analyzed for the selected dates before earthquakes of interest. The Spatio-temporal changes of Temperature around the epicenter were managed considering 270km impact area. Figure 4 reveals the spatial and temporal variations of MODIS average temperature around the epicenter of 8^{th} September Mexico earthquake 2017 for significant dates. Meanwhile, figure 5 indicated statistical analysis of temperature during the period from 1^{st} June to 1^{st} October 2017. Concerning the behaviour of the mean LST obtained, the high values were observed more times on (5^{th} June 2017) followed by decreasing in temperature few days before the two large earthquakes on 14^{th} with Mw = 6.9 and 22^{nd} June 2017 with Mw = 6.8, (on 24^{th} June 2017 and 9^{th} August 2017). High dramatic decrease in LST values is observed few days before the mainshock. Based on the $\pm 2\sigma$ rule, the day (24^{th} June 2017) represented as anomalous day before main-shock. After the main-shock, a disturbance in the Mean values is observed due the aftershocks.

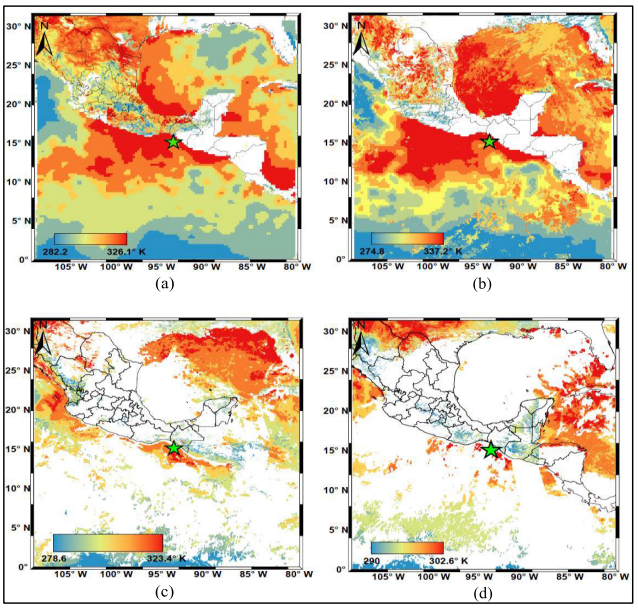

FIGURE 4. MODIS average temperature around the epicenter of 8th September Mexico earthquake 2017 for these selected dates, a) 21st June 2017, b) 24th June 2017, c) 7th July 2017, d) 5th September 2017. The epicenter is denoted by green star.

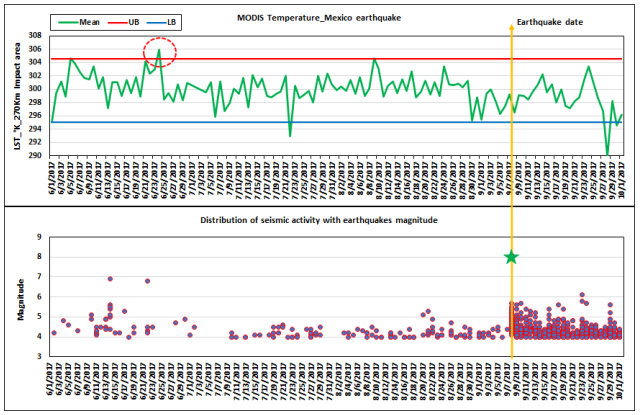

FIGURE 5. Statistical analysis indicated the thermal anomaly within 270 Km impact area around the epicenter of September, 08 Mexico earthquake 2017 with the distribution of seismic activity. The red circle indicated the thermal anomaly.

Figure 6 shows the MERRA-2 SAT difference map on the day of 21st June 2017 with respect to the historical mean computed on the last 10 years around Mexico area. The epicenter is represented by green star.

B. SECOND CASE STUDY (15 APRIL 2016 Mw = 7 JAPAN EQ)

Figure 7 depicts the anomalous space magnetic field event that is measured by the Swarm A satellite on 21st March 2016, about 25 days before the 15th April 2016 Mw = 7 Japan EQ with epicenter at 32.791°N 130.754°E. This magnetic field anomaly is powerful and unexpected at the nighttime (mean LT=22:13 MLT) at low geomagnetic indices (Dst = −9nT).

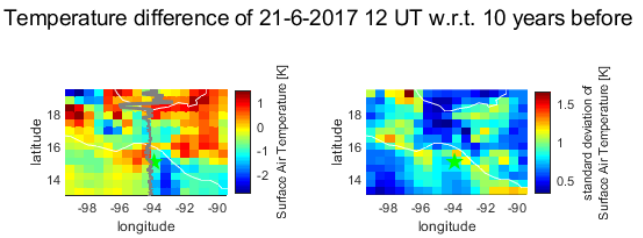

FIGURE 6. MERRA-2 Surface Air Temperature difference map on the day of 21st June 2017 with respect to the historical mean computed on the last 10 years around Mexico area. The epicenter is represented by green star. The Swarm magnetic residuals are superposed as grey line for comparison.

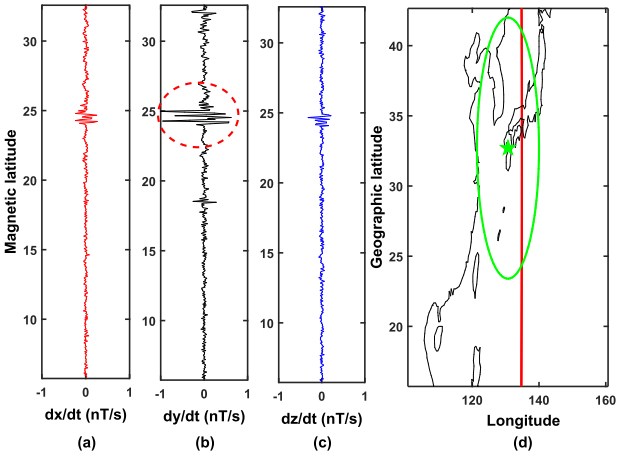

FIGURE 7. Magnetic variation detected by AMSW algorithm on 21st March 2016 at Swarm A, i.e., 25 days before the 15th April 2016 Mw = 7 Japan EQ.

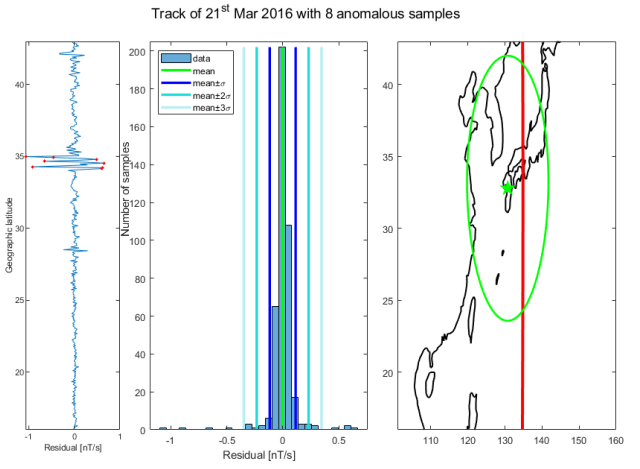

FIGURE 8. Residual of Y component of magnetic field of Swarm Alpha on 21st March 2016 around M7.0 Japan earthquake. A geographical map with red projection of the track and the histogram of the residuals are represented.

Residual of Y component of magnetic field of SW-A on 21st March 2016 around M7.0 Japan earthquake is shown in figure 8. A geographical map with red projection of the track and the histogram of the residual are represented.

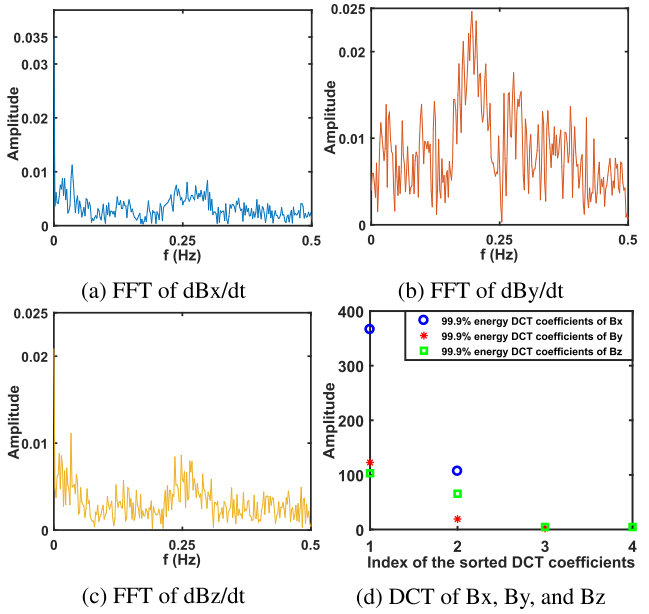

FIGURE 9. Spectral analysis output confirms the anomalous event detected by AMSW algorithm in figure 7.

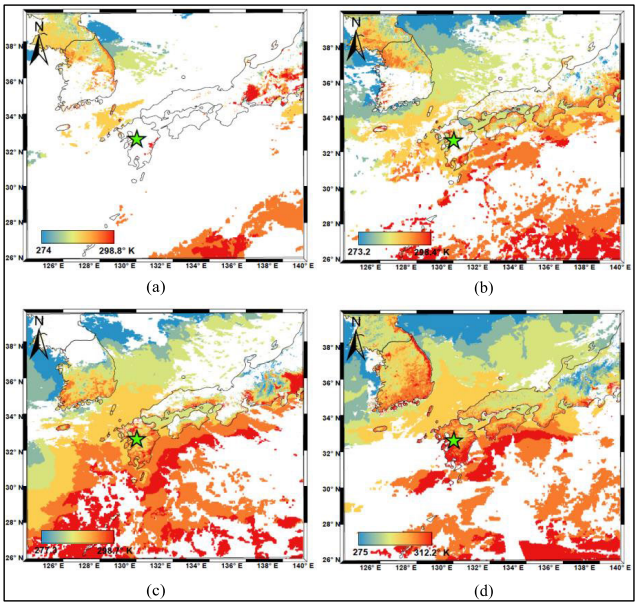

FIGURE 10. MODIS average temperature around the epicenter of April, 15 Japan earthquake 2016 for these selected dates, a) 23th February 2016, b) 26th February 2016, c) 2nd March 2016, and d) 21st March 2016. The epicenter is denoted by green star.

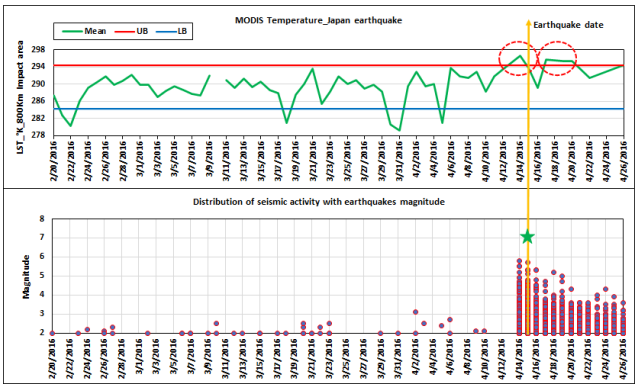

FIGURE 11. Statistical analysis indicated the thermal anomaly within 800 Km impact area around the epicenter of April, 15th Japan earthquake 2016 with the distribution of seismic activity. The red circle indicated the thermal anomaly.

Particularly, we show the obtained results from the AMSW algorithm, FFT transform, and DCT transform. The anomaly can be clearly identified from the AMSW algorithm of the B_y and its corresponding frequency spectrum. Furthermore, the DCT transform can identify the event for all magnetic field components B_x, B_y, and B_z, where each can be represented by only 2, 3, and 4 DCT coefficients for B_x, B_y, and B_z components, respectively as depicted in figure 9d.

Regarding LST and SST in the case of Japan earthquake, The Spatio-temporal changes in temperature around the epicenter were managed considering 800km impact area. The figure 10 reveals the spatial and temporal variations of MODIS average temperature around the epicenter of April, 15th Japan earthquake 2016 for significant dates. While the figure 11 indicated statistical analysis of temperature during the period from 20th February 2016 to 26th April 2016. Concerning the behaviour of the mean LST obtained, the highest values were observed on (21st March 2016) followed by abnormal decreasing in temperature through 10-15 days before the main-shock. The anomalous days were observed; one day before and the main-shock on 14th April and two days after the main-shock on 17th and 20th April 2016. The results of values are ranging from low (deep blue) to high (Red) in Kelvin around the epicenter. The spatial distribution of Mean trend is characterized by thermal anomaly from 14−21 April 2016 due to accumulation of stress which lead to foreshocks of large earthquakes before the main-shock and the swarm of aftershock that recorded close and around the epicenter.

Figure 12 shows the MERRA-2 Surface Air Temperature difference map on the day of 21st March 2016 with respect to the historical mean computed on the last 10 years around Japan islands and Korean Peninsula. The epicenter is represented by green star. It is noteworthy that, in the case of this earthquake, although no anomalies are observed by both magnetic swarm and LST methodologies around the epicenter, an anomaly is clearly observed by the DCT.

C. THIRD CASE STUDY (1 APRIL 2014 Mw = 8.2 CHILE EARTHQUAKE)

On the 1st of April 2014, EQ (Mw = 8.2) occurred in 94 km NW of Iquique, Chile (19.610° S and 70.769° W). The time of the EQ was late at 23:46:47 (UTC) with 25.0 km depth. The Swarm A satellite measured an anomalous magnetic event on 5th March 2014 (mean UTC=10:24, mean LT=5:22, Dst=−10nT) as shown in figure 13. De Santis *et al.* [35] noticed

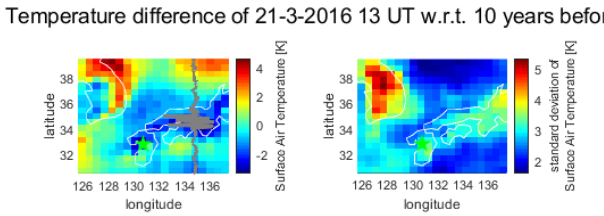

FIGURE 12. MERRA-2 Surface Air Temperature difference map on the day of 21st March 2016 with respect to the historical mean computed on the last 10 years around Japan islands and Korean Peninsula. The epicenter is represented by green star. The Swarm magnetic residuals are superposed as grey line for comparison.

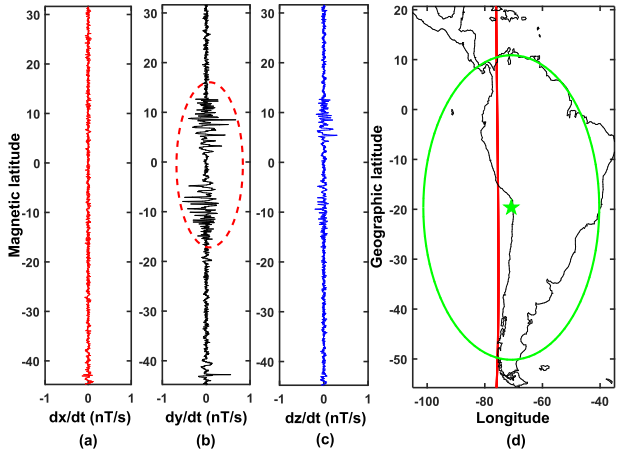

FIGURE 13. Magnetic variation detected by AMSW algorithm on 5th March 2014 at Swarm A, i.e., 25 days before the 1st April 2014 Mw = 8.2 Chile EQ.

that the two anomalies appear above the epicenter and in its conjugate point. Although we cannot exclude completely an EIA (Equatorial Ionospheric Anomaly), which is more typical in daytime, the early time in the morning of LT tends to favor a precursory ionospheric signal.

Figure 14 shows the residual of Y component of magnetic field of SW-A on 5th March 2014 around M8.2 Chile earthquake. A geographical map with red projection of the track and the histogram of the residual are represented. As shown in figure 15, the anomaly is identified clearly from the AMSW analysis of the B_y, and its corresponding frequency spectrum. Moreover, from the DCT transforms of the B_x, B_y, and B_z, we can significantly recognize the presence of the anomalous event.

In the case of Chile earthquake, The Spatio-temporal changes in temperature around the epicenter were managed considering 600km impact area. Figure 16 reveals the spatial and temporal variations of MODIS average temperature around the epicenter of April, 1st Iquique, Chile earthquake 2014 for significant dates. While figure 17 indicated statistical analysis of temperature during the period from 1st February 2014 to 10th April 2014. Concerning the behaviour of the mean LST obtained, the highest value (even if it doesn't overpass the upper threshold) was observed on

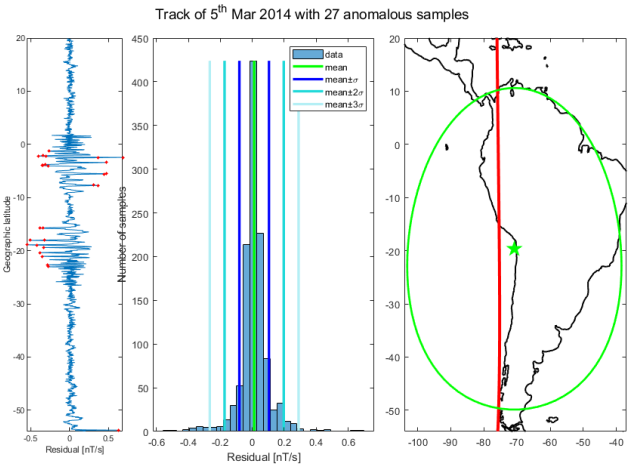

FIGURE 14. Residual of Y component of magnetic field of Swarm Alpha on 5th March 2014 around M8.2 Chile earthquake. A geographical map with red projection of the track and the histogram of the residuals are represented.

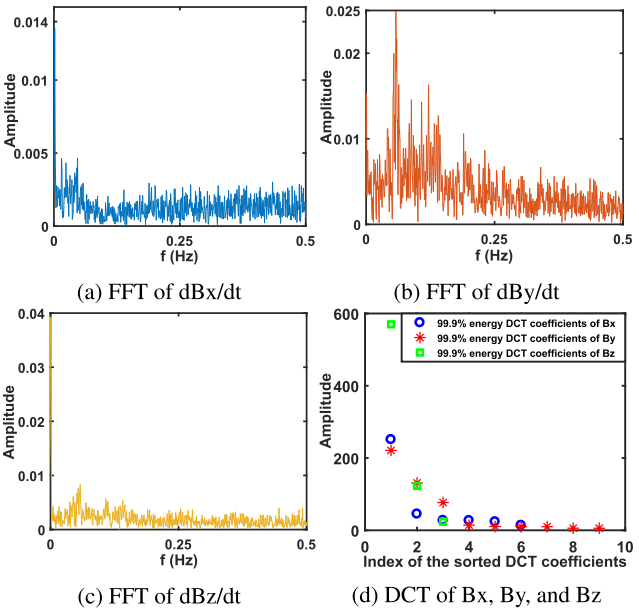

FIGURE 15. Spectral analysis output confirms the anomalous event detected by AMSW algorithm in figure 13.

(21st March 2016) followed by abnormal decreasing in temperature within 8 days before the main-shock. Figure 18 shows MERRA-2 Surface Air Temperature difference map on the day of 5th March 2014 with respect to the historical mean computed on the last 10 years around Chile and northern area. The epicenter is represented by green star.

D. FOURTH CASE STUDY (28 SEPTEMBER 2018 Mw = 7.5 PALU, INDONESIA)

This case study considers the EQ occurred on 28th September 2018 in Palu, Indonesia at 10:02:45 (UTC) 0.256° S and 119.846° E with a depth of 13.5 km. SW-A detected magnetic variations on 2nd August 2018 (i.e., 57 days before the EQ) as

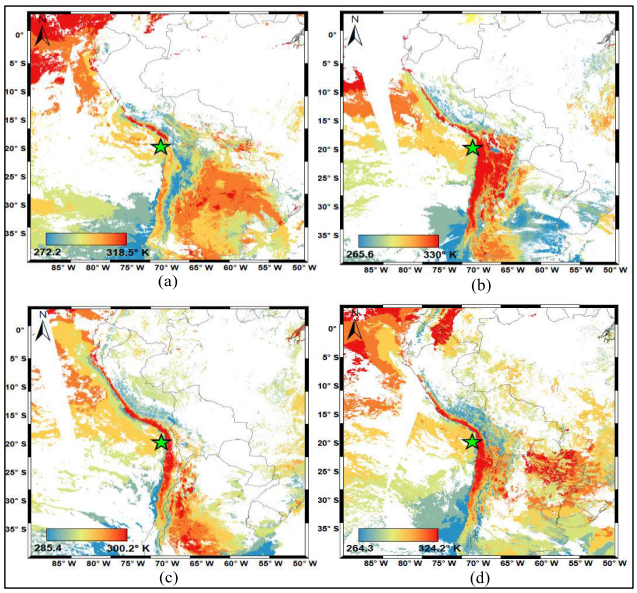

FIGURE 16. MODIS average temperature around the epicenter of April, 1st Iquique, Chile earthquake 2014 for these selected dates, a) 5th March 2014, b) 21st March 2014, c) 28th March 2014, and d) 1st April 2014. The epicenter is denoted by green star.

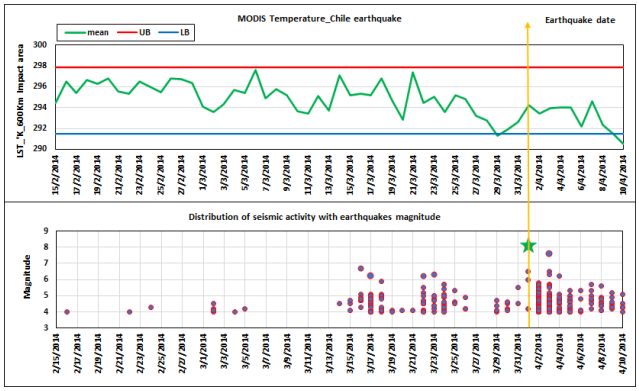

FIGURE 17. Statistical analysis indicated the thermal anomaly within 600 Km impact area around the epicenter of 1st April 2014, Iquique, Chile earthquake with the distribution of seismic activity.

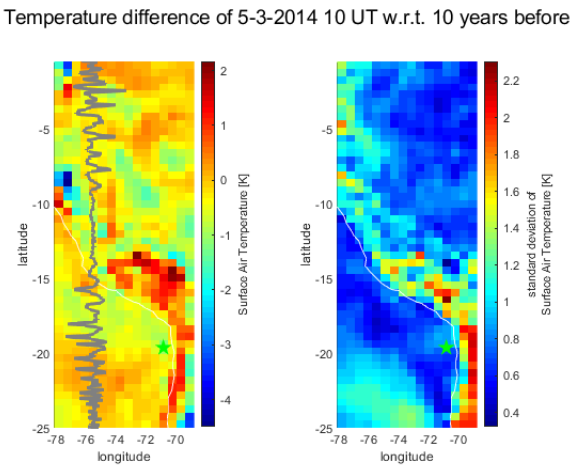

FIGURE 18. MERRA-2 Surface Air Temperature difference map on the day of 5th March 2014 with respect to the historical mean computed on the last 10 years around Chile and northern area. The epicenter is represented by green star.The Swarm magnetic residuals are superposed as grey line for comparison.

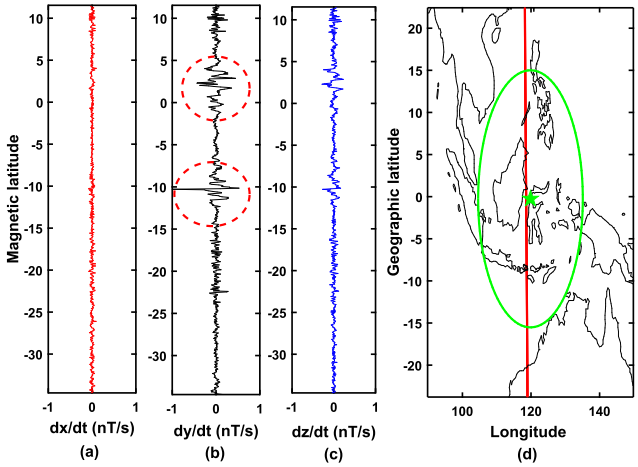

FIGURE 19. Magnetic variation detected by AMSW algorithm on 2nd August 2018 at Swarm A, i.e., 57 days before the 28th September 2018 Mw = 7.5 Indonesia EQ.

depicted in figure 19 (mean UTC=20:48, mean LT=04:42, Dst=5nT). Figure 20 shows the residual of Y component of magnetic field of SW-A on 2nd August 2018 around M7.5 Indonesia earthquake. A geographical map with red projection of the track and the histogram of the residual are represented.

Without lose of generality, using FFT transform, and DCT transform, in figure 21, we depict the anomaly from the AMSW algorithm of the B_y and its corresponding frequency spectrum. Moreover, the DCT transform can identify the event for all magnetic field components B_x, B_y, and B_z, where each can be represented by only 4 to 15 DCT coefficients for B_x, B_y, and B_z components.

In the case of Palu, Indonesia earthquake, with intensity value IX, The Spatio-temporal changes in temperature around the epicenter were managed considering 600km impact area. Figure 22 reveals the spatial and temporal variations of MODIS average temperature around the epicenter of September, 28th Palu, Indonesia earthquake 2018 for significant dates. While figure 23 indicated statistical analysis of temperature during the period from 1st August 2018 to 28th October 2018. Concerning the behaviour of the mean of the temperature obtained, the high values were observed more than two weeks before the main-shock on (4th, 6th and 11th September, 2018) followed by abnormal decreasing in temperature five days before main-shock. The results of LST values are ranging from low (deep blue) to high (Red) in Kelvin around the epicenter. This anomaly is compatible with low geomagnetic anomaly as well as anomalous retrieved from the DCT transform. Figure 24 shows the

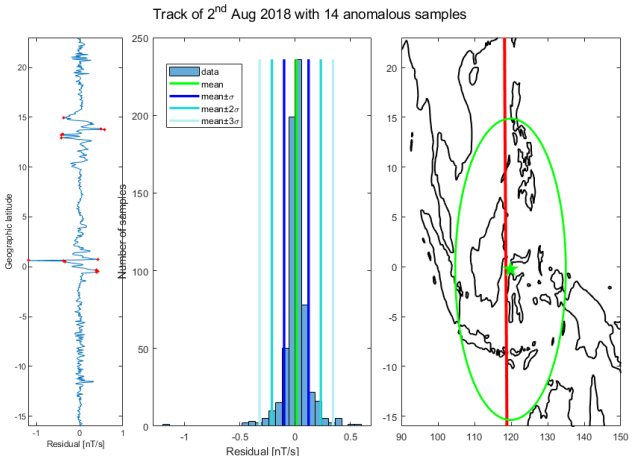

FIGURE 20. Residual of Y component of magnetic field of Swarm Alpha on 2nd August 2018 around M7.5 Indonesia earthquake. The histogram of the residuals is represented too and a geographical map with the Red projection of the track.

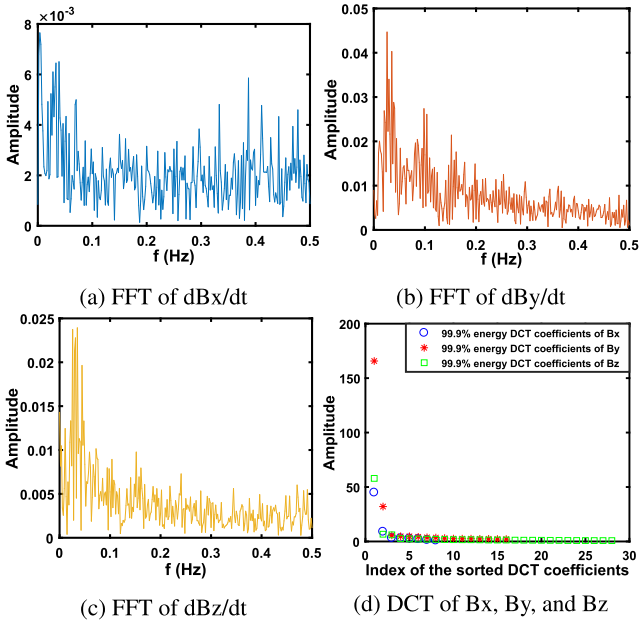

FIGURE 21. Spectral analysis output confirms the anomalous event detected by AMSW algorithm in Figure 19.

MERRA-2 SAT difference map on the day of 2nd August 2018 with respect to the historical mean computed on the last 10 years around Indonesia archipelago. The epicenter is represented by green star.

E. FIFTH CASE STUDY (2nd MARCH 2016 Mw = 7.8 INDONESIA-SUMATRA)

This case study considers the EQ occurred on 2nd March 2016 in Southwest of Sumatra, Indonesia at 12:49:48 (UTC) 4.952° S and 94.330° E with a depth of 24.0 km. SW-A detected magnetic variations on 14th February 2016 (i.e., 16 days before the EQ), as depicted in figure 25 (mean UTC=18:17, mean LT=01:20, Dst= −9nT). Figure 26

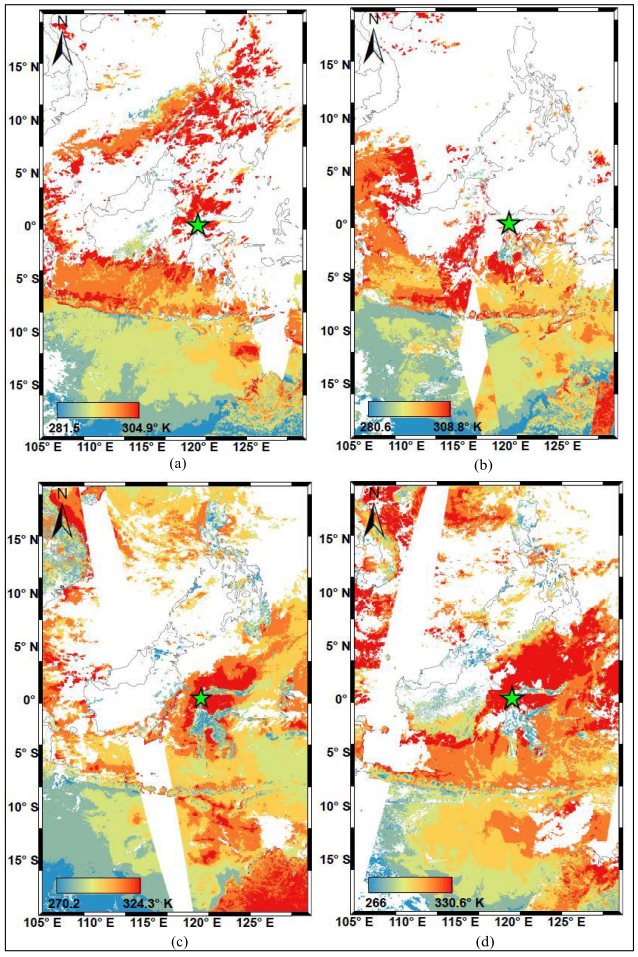

FIGURE 22. MODIS average temperature around the epicenter of September, 28th Palu, Indonesia earthquake 2018 for these selected dates, a) 2nd August 2018, b) 25th August 2018, c) 26th September 2018, and d) 27th September 2018. The epicenter is denoted by green star.

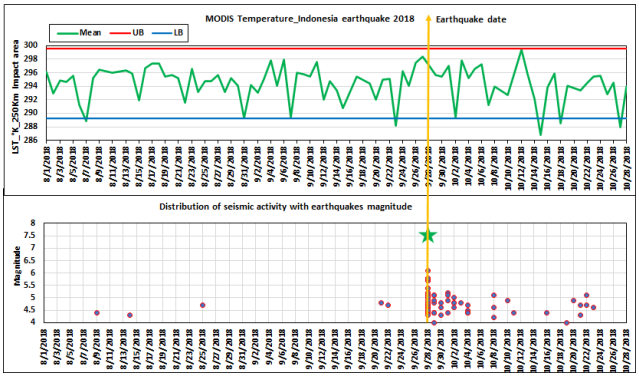

FIGURE 23. Statistical analysis indicated the thermal anomaly within 250 Km impact area around the epicenter of September, 28th Palu, Indonesia earthquake 2018 with the distribution of seismic activity.

shows the residual of Y component of magnetic field of SW-A on 14th February 2016 around M7.8 Sumatra, Indonesia earthquake. A geographical map with red projection of the track and the histogram of the residual are represented.

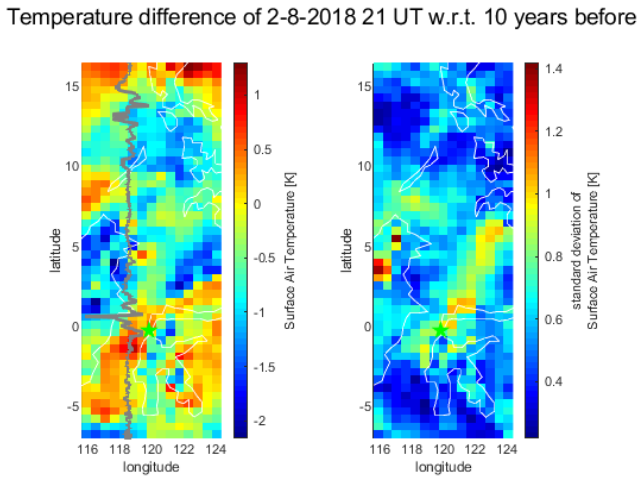

FIGURE 24. MERRA-2 Surface Air Temperature difference map on the day of 2^{nd} August 2018 with respect to the historical mean computed on the last 10 years around Indonesia archipelago. The epicenter is represented by green star. The Swarm magnetic residuals are superposed as grey line for comparison.

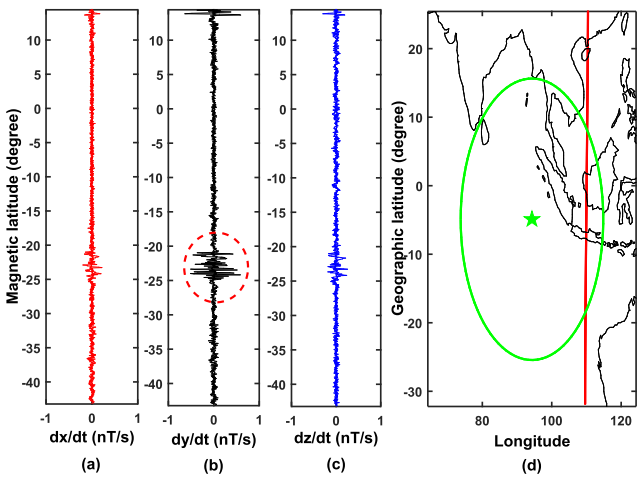

FIGURE 25. Magnetic variation detected by AMSW algorithm on 14^{th} February 2016 at SW-A, i.e., 16 days before the 2^{nd} March 2016 Mw = 7.8 Indonesia-Sumatra EQ.

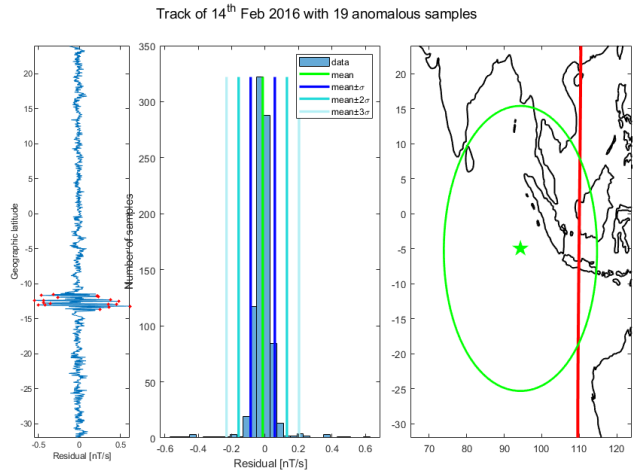

FIGURE 26. Residual of Y component of magnetic field of SW-A on 14^{nd} February 2016 around M7.8 Sumatra-Indonesia earthquake. A geographical map with red projection of the track and the histogram of the residuals are represented.

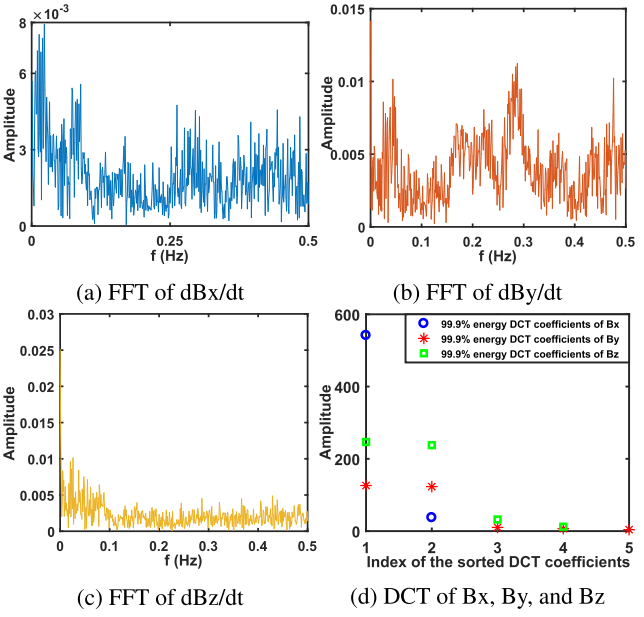

FIGURE 27. Spectral analysis output confirms the anomalous event detected by AMSW algorithm in figure 25.

The magnetic variation can be identified from $\frac{dB_x}{dt}$, $\frac{dB_y}{dt}$, and $\frac{dB_z}{dt}$, their FFT transforms, and their DCT transforms as shown in figure 27.

The Spatio-temporal changes in temperature around the epicenter were managed considering 600km impact area. Figure 28 reveals the spatial and temporal variations of MODIS average temperature around the epicenter of March, 2^{nd} Sumatra, Indonesia earthquake 2016 for significant dates. While the figure 29 indicated statistical analysis of temperature during the period from 15^{th} January 2016 to five days after the earthquake. Concerning the behaviour of the mean LST obtained, the highest values were observed on (18^{th} and 23^{rd} February 2016) followed by decreasing in temperature one week before the main-shock. Both days present values above the upper threshold and not associate with any M5+ earthquake on the same day, so potentially good candidate to be precursor of M7.8 Sumatra earthquake. The results of LST values are ranging from low (deep blue) to high (Red) in Kelvin around the epicenter. Figure 30 shows the MERRA-2 SAT difference map on the day of 14^{th} February 2016 with respect to the historical mean computed on the last 10 years around Indonesia-Sumatra Islands. The epicenter is represented by green star. It is noteworthy that, in the case of Sumatra, Indonesia earthquake, although no anomalies are observed by both magnetic swarm and LST methodologies around the epicenter, an anomaly is clearly observed by the DCT methodology.

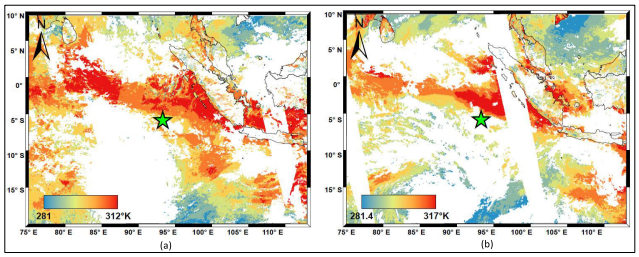

FIGURE 28. MODIS average temperature around the epicenter of March, 2nd Sumatra, Indonesia earthquake 2016 for these selected dates, a) 14th February 2016, and b) 15th February 2016. The epicenter is denoted by green star.

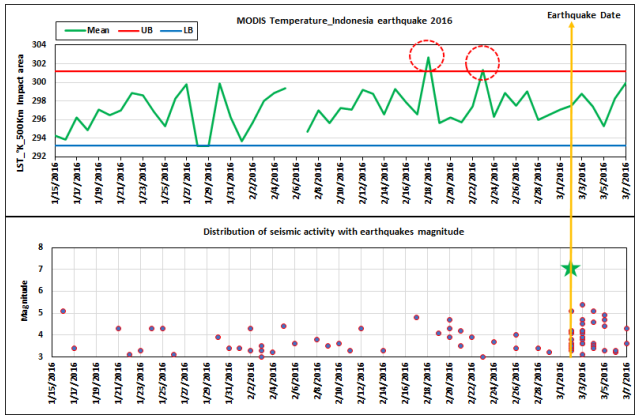

FIGURE 29. Statistical analysis indicated the thermal anomaly within 500 Km impact area around the epicenter of March, 2nd Sumatra, Indonesia earthquake 2016 with the distribution of seismic activity. The red circle indicated the thermal anomaly.

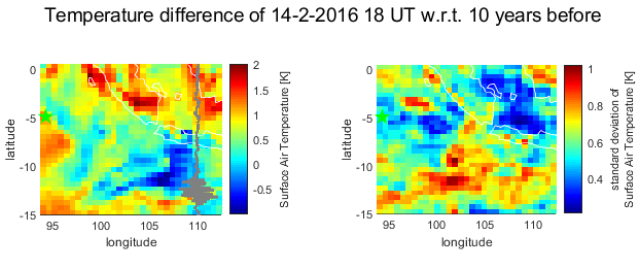

FIGURE 30. MERRA-2 Surface Air Temperature difference map on the day of 14th February 2016 with respect to the historical mean computed on the last 10 years around Indonesia-Sumatra Islands. The epicenter is represented by green star. The Swarm magnetic residuals are superposed as grey line for comparison.

V. COMPARISON OF THE RESULTS

Based on the simultaneous analyses of the satellite magnetic data along with the temperature data, it is possible to compare the five case studies. We underline an increment of temperatures (i.e., surface ground warming) in the same area of the magnetic anomaly for some of the case studies. In the case of M8.2 Mexico 2017 (an anomaly of surface warming is observed around and close the epicenter in a compatible position between magnetic and temperature data: Figures 2, 4, and 6). Likewise, there is an increase in the

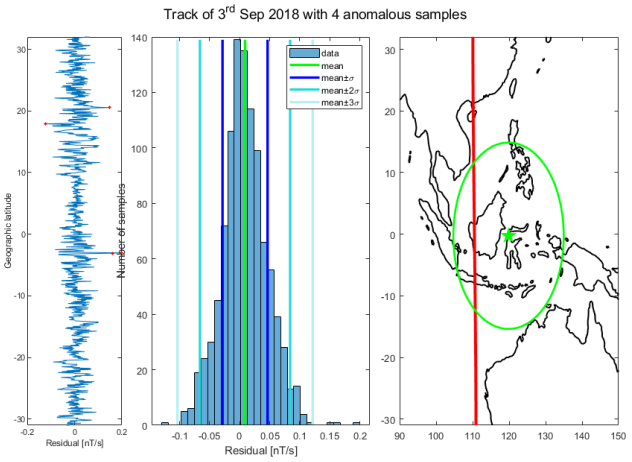

FIGURE 31. Residual of Y component of magnetic field of Swarm Alpha on 3rd September 2018 around M7.5 Indonesia earthquake. A geographical map with red projection of the track and the histogram of the residuals are represented.

temperature Northern the M8.2 Chile 2014 EQ (at least for the first anomaly that coincides with a higher temperature in a wide region: 74° W ∼ 71° W longitude, 20° S ∼ 13° S latitude, as shown in figures: 13, 15, and 17, in the case of M7.5 Indonesia 2018 EQ (warmed area at south-west and close with respect to the epicenter as depicted in figure 22 24 very close to the magnetic anomaly of figure 20. In the case of M8.2 Mexico 2017 earthquake there is warming just western of the earthquake but it is not significant as the normal variation of the region is higher as underlined in the standard deviation map obtained form MERRA-2 SAT data. Furthermore, the LST and SST values show significant large anomaly at the location of the magnetic swarm anomaly (figures 1 and 4 case studies of M7.0 Japan 2016 and M7.8 Sumatra-Indonesia 2016 earthquakes don't show a warming in the location of the magnetic anomaly. Furthermore, the LST and SST values show low anomaly at the location of the magnetic swarm anomaly (figures: 7, 10, 25 and 28). Our results indicated that, the behavior of MODIS temperature before large earthquakes in most cases is characterized by increasing in temperature (positive anomaly) following by decrease or abnormal (negative anomaly) with respect to the Mean trend in temperature within one - two weeks before the main-shock. We would like to emphasis here that, the integration of EQs precursors is a very interesting topic that definitely needs more investigations so that robust correlations among the considered precursors can be verified for different land/sea locations.

Finally a comparison in the area of the M7.5 Indonesia 2018 EQ with a magnetic track without any visual anomaly is shown in figure 31. This track has only 4 anomalous samples (i.e., the samples that are out of 3σ of the distribution) which are much less than case studies with a visual magnetic anomaly (number of anomalous samples are 29, 8, 27, 14, and 19 in figures 2, 8, 14, 20 and 26, respectively) confirming by an objective criteria that the anomalies are presented and properly defined (i.e., with more than 5 anomalous samples).

We extract the anomalous track for the M7.8 Sumatra-Indonesia earthquake (fifth case study) starting from three months before the event. Figures S1-S8 in the Supplementary Materials show a selection of four most interesting tracks in SW−A preceding the event along with SAT maps of the same days. We do not find interest tracks in SW−B, while in SW−C, there are some interesting tracks but almost coincide with SW−A. Therefore, to avoid the redundancy, we do not select them. More details are provided in the Supplementary Materials. Furthermore, we made a confutation analysis by analyzing one month before the same area of the four events (1^{st}, 2^{nd}, 4^{th} and 5^{th}) where no shallow (depth $\leq$ 50 km) M5.5+ earthquakes happened. Regarding the 3rd event, we did not find a month, which has an earthquake with Mw=5.5+ before the EQ, till the starting date of Swarm mission (November 2013). Figures S9−S32, in the supplementary materials, show the results obtained applying AMSW algorithms to the magnetic field data with the same conditions for the real cases. Also, figures S33−S36, show MODIS average temperatures around the epicenter of the earthquakes for some selected dates as the same used for magnetic tracks without anomaly observed. It is clear from the confutation analysis that no specific features of the Y component of magnetic field.

We highlight here that the integration of multiple precursors methods is beneficial in identifying the anomalies, which precede large EQs. In some case studies, the anomalies might be more clear with some methods and barely identifiable with others. It is worth mentioning that the FFT and DCT methods have proven beneficial for showing the anomalies in the above mentioned five case studies.

VI. CONCLUSION

In this work, we considered the analysis of space magnetic anomalous events that can precede large EQs. Specifically, we used AMSW algorithm, FFT transform and DCT transform to get insights about these magnetic anomalous events. Besides, the LST and SST values were retrieved from Moderate Resolution Imaging Spectroradiometer (MODIS) Aqua and Terra satellites data for the selected earthquakes. Moreover, SAT from Modern-Era Retrospective analysis for Research and Applications, Version 2 (MERRA-2) is used. This work highlighted the potential of using remote sensing data as precursors data to explore earthquake signals and variation in the dynamics of thermal conditions around epicenters and in the fault area. It is clear that space magnetic and temperature anomalies can be identified. We emphasize here that our analyses could identify anomalous events of magnetic field, LST and SAT before the EQ by periods that can reach 80 days. The relationships between the seismo-ionospheric phenomena and their interrelations with ground magnetic stations would be the subject of further studies and represent the first step for EQs prediction depending on the monitoring of space magnetic and temperature anomalies. In the future work, we aim to consider different case studies of EQs with similar magnitude and depth.

ACKNOWLEDGMENT

The authors thank the European Space Agency (ESA) for providing the Swarm data which can be accessed freely from the Swarm website: ftp://swarm-diss.eo.esa.int. They also thank USGS organization for providing MODIS V6 product data. The MODIS data can be downloaded from https://earthexplorer.usgs.gov and https://lpdaacsvc.cr.usgs.gov. They also thank LIMADOU-Science project funded by Italian Space Agency. This work was supported by JSPS KAKENHI under Grant JP20H01961 and Grant JP15H05815.

REFERENCES

[1] T. Maruyama, T. Tsugawa, H. Kato, A. Saito, Y. Otsuka, and M. Nishioka, "Ionospheric multiple stratifications and irregularities induced by the 2011 off the pacific coast of Tohoku earthquake," *Earth, Planets Space*, vol. 63, no. 7, pp. 869–873, Jul. 2011.

[2] J.-Y. Liu, C.-H. Chen, C.-H. Lin, H.-F. Tsai, C.-H. Chen, and M. Kamogawa, "Ionospheric disturbances triggered by the 11 March 2011 M9.0 Tohoku earthquake," *J. Geophys. Res. Space Phys.*, vol. 116, no. A6, 2011, Art. no. A06319.

[3] S. A. Pulinets, A. D. Legen'ka, V. A. Alekseev, "Pre-earthquake ionospheric effects and their possible mechanisms," in *Dusty and Dirty Plasmas, Noise, and Chaos in Space and in the Laboratory*, H. Kikuchi, Ed. Boston, MA, USA: Springer, 1994, doi: 10.1007/978-1-4615-1829-7_46.

[4] S. Pulinets, V. Khegaj, K. Boyarchuk, and A. Lomonosov, "Atmospheric electric field as a source of ionospheric variability," *Uspekhi Fizicheskikh Nauk*, vol. 168, no. 5, pp. 582–589, 1998.

[5] S. A. Pulinets, K. A. Boyarchuk, V. V. Hegai, V. P. Kim, and A. M. Lomonosov, "Quasielectrostatic model of atmosphere-thermosphere-ionosphere coupling," *Adv. Space Res.*, vol. 26, no. 8, pp. 1209–1218, Jan. 2000.

[6] I. Mahmood, M. F. Iqbal, M. I. Shahzad, and S. Qaiser, "Investigation of atmospheric anomalies associated with kashmir and awaran earthquakes," *J. Atmos. Solar-Terr. Phys.*, vol. 154, pp. 75–85, Feb. 2017.

[7] F. Freund, "Pre-earthquake signals: Underlying physical processes," *J. Asian Earth Sci.*, vol. 41, nos. 4–5, pp. 383–400, Jun. 2011.

[8] F. Freund, "Earthquake forewarning—A multidisciplinary challenge from the ground up to space," *Acta Geophysica*, vol. 61, no. 4, pp. 775–807, Aug. 2013.

[9] M. Hayakawa, T. Horie, F. Muto, Y. Kasahara, K. Ohta, J.-Y. Liu, and Y. Hobara, "Subionospheric VLF/LF probing of ionospheric perturbations associated with earthquakes: A possibility of earthquake prediction," *SICE J. Control, Meas., Syst. Integr.*, vol. 3, no. 1, pp. 10–14, Jan. 2010.

[10] S. Pulinets and D. Ouzounov, "Lithosphere–Atmosphere–Ionosphere coupling (LAIC) model—An unified concept for earthquake precursors validation," *J. Asian Earth Sci.*, vol. 41, nos. 4–5, pp. 371–382, Jun. 2011.

[11] F. Di Luccio, G. Ventura, R. Di Giovambattista, A. Piscini, and F. Cinti, "Normal faults and thrusts reactivated by deep fluids: The 6 April 2009 M_w 6.3 L'Aquila earthquake, central Italy," *J. Geophys. Res. Solid Earth*, vol. 115, no. B6, 2010, Art. no. B06315.

[12] D. Ouzounov, V. Tramutoli, S. Pulinets, T. Liu, C. Filizzola, N. Genzano, M. Lisi, L. Petrov, and M. Kafatos, "Multi-sensor integration of space and ground observations of pre-earthquake anomalies associated with M6.0, August 24, 2014 Napa, California," in *Proc. EGUGA*, 2015, p. 6014.

[13] S. A. Pulinets, D. P. Ouzounov, A. V. Karelin, and D. V. Davidenko, "Physical bases of the generation of short-term earthquake precursors: A complex model of ionization-induced geophysical processes in the lithosphere-atmosphere-ionosphere-magnetosphere system," *Geomagnetism Aeronomy*, vol. 55, no. 4, pp. 521–538, Jul. 2015.

[14] W. H. Prescott, "Pre-earthquake processes: A multidisciplinary approach to earthquake prediction studies," *Int. Geol. Rev.*, vol. 61, no. 16, pp. 2080–2082, Nov. 2019, doi: 10.1080/00206814.2019.1579001.

[15] I. Mahmood, M. F. Iqbal, and M. I. Shahzad, "Precursor anomalies prior to the 2006 java and 2016 Yujing earthquakes," *J. Geophys. Eng.*, vol. 15, no. 4, pp. 1506–1516, Aug. 2018.

[16] I. Mahmood, "Anomalous variations of air temperature prior to earthquakes," *Geocarto Int.*, pp. 1–13, Aug. 2019, doi: 10.1080/10106049.2019.1648565.

[17] S. Chen, J. Ma, L. Liu, and P. Liu, "An enhancive phenomenon of thermal infrared radiation prior to Pakistan earthquake," (in Chinese), *Progress Natural Sci.*, vol. 16, no. 11, pp. 1487–1490, 2006.

[18] S. Choudhury, S. Dasgupta, A. K. Saraf, and S. Panda, "Remote sensing observations of pre-earthquake thermal anomalies in Iran," *Int. J. Remote Sens.*, vol. 27, no. 20, pp. 4381–4396, Oct. 2006.

[19] A. K. Saraf, V. Rawat, P. Banerjee, S. Choudhury, S. K. Panda, S. Dasgupta, and J. D. Das, "Satellite detection of earthquake thermal infrared precursors in Iran," *Natural Hazards*, vol. 47, no. 1, pp. 119–135, Oct. 2008.

[20] A. Saraf and S. Choudhury, "Cover: NOAA-AVHRR detects thermal anomaly associated with the 26 January 2001 Bhuj earthquake, Gujarat, India," *Int. J. Remote Sens.*, vol. 26, no. 6, pp. 1065–1073, 2005.

[21] A. A. Tronin, "Thermal IR satellite sensor data application for earthquake research in China," *Int. J. Remote Sens.*, vol. 21, no. 16, pp. 3169–3177, Jan. 2000.

[22] A. Bhardwaj, S. Singh, L. Sam, P. K. Joshi, A. Bhardwaj, F. J. Martín-Torres, and R. Kumar, "A review on remotely sensed land surface temperature anomaly as an earthquake precursor," *Int. J. Appl. Earth Observ. Geoinformation*, vol. 63, pp. 158–166, Dec. 2017.

[23] M. Hayakawa and O. A. Molchanov, *Seismo Electromagnetics: Lithosphere-Atmosphere-Ionosphere Coupling*. Tokyo, Japan: TERRAPUB, 2002.

[24] M. Blackett, M. J. Wooster, and B. D. Malamud, "Exploring land surface temperature earthquake precursors: A focus on the Gujarat (India) earthquake of 2001," *Geophys. Res. Lett.*, vol. 38, no. 15, Aug. 2011, Art. no. L15303.

[25] V. Tramutoli, C. Aliano, R. Corrado, C. Filizzola, N. Genzano, M. Lisi, G. Martinelli, and N. Pergola, "On the possible origin of thermal infrared radiation (TIR) anomalies in earthquake-prone areas observed using robust satellite techniques (RST)," *Chem. Geol.*, vol. 339, pp. 157–168, Feb. 2013.

[26] W. H. Prescott, *Pre-Earthquake Processes: A Multidisciplinary Approach to Earthquake Prediction Studies*. 2019.

[27] D. Ouzounov, S. Pulinets, K. Hattori, and P. Taylor, *Pre-Earthquake Processes: A Multidisciplinary Approach to Earthquake Prediction Studies*, vol. 234. Hoboken, NJ, USA: Wiley, 2018.

[28] M. Parrot *et al.*, "Atmospheric and ionospheric coupling phenomena associated with large earthquakes," *Eur. Phys. J. Spec. Top.*, vol. 230, pp. 197–225, 2021, doi: 10.1140/epjst/e2020-000251-3.

[29] D. Ouzounov, S. Pulinets, A. Romanov, A. Romanov, K. Tsybulya, D. Davidenko, M. Kafatos, and P. Taylor, "Atmosphere-ionosphere response to the m9 tohoku earthquake revealed by multi-instrument space-borne and ground observations: Preliminary results," *Earthq. Sci.*, vol. 24, no. 6, pp. 557–564, Dec. 2011.

[30] F. Masci, J. N. Thomas, F. Villani, J. A. Secan, and N. Rivera, "On the onset of ionospheric precursors 40 min before strong earthquakes," *J. Geophys. Res. Space Phys.*, vol. 120, no. 2, pp. 1383–1393, Feb. 2015.

[31] K. Rawer, *Wave Propagation in the Ionosphere*, vol. 5. Springer, 2013, doi: 10.1007/978-94-017-3665-7.

[32] M. C. Kelley, *The Earth's Ionosphere: Plasma Physics and Electrodynamics*. New York, NY, USA: Academic, 2009.

[33] E. Friis-Christensen, H. Lühr, D. Knudsen, and R. Haagmans, "Swarm—An Earth observation mission investigating geospace," *Adv. Space Res.*, vol. 41, no. 1, pp. 210–216, Jan. 2008.

[34] F. Freund, G. Ouillon, J. Scoville, and D. Sornette, "Earthquake precursors in the light of peroxy defects theory: Critical review of systematic observations," 2017, *arXiv:1711.01780*. [Online]. Available: http://arxiv.org/abs/1711.01780

[35] A. De Santis, D. Marchetti, L. Spogli, G. Cianchini, F. J. Pavón-Carrasco, G. D. Franceschi, R. Di Giovambattista, L. Perrone, E. Qamili, C. Cesaroni, A. De Santis, A. Ippolito, A. Piscini, S. A. Campuzano, D. Sabbagh, L. Amoruso, M. Carbone, F. Santoro, C. Abbattista, and D. Drimaco, "Magnetic field and electron density data analysis from swarm satellites searching for ionospheric effects by great earthquakes: 12 case studies from 2014 to 2016," *Atmosphere*, vol. 10, no. 7, p. 371, Jul. 2019.

[36] D. Marchetti and M. Akhoondzadeh, "Analysis of swarm satellites data showing seismo-ionospheric anomalies around the time of the strong mexico (Mw = 8.2) earthquake of 08 september 2017," *Adv. Space Res.*, vol. 62, no. 3, pp. 614–623, Aug. 2018.

[37] D. Marchetti, A. De Santis, S. D'Arcangelo, F. Poggio, S. Jin, A. Piscini, and S. A. Campuzano, "Magnetic field and electron density anomalies from swarm satellites preceding the major earthquakes of the 2016–2017 Amatrice-Norcia (Central Italy) seismic sequence," *Pure Appl. Geophys.*, vol. 177, no. 1, pp. 305–319, Jan. 2020.

[38] G. Balasis and M. Mandea, "Can electromagnetic disturbances related to the recent great earthquakes be detected by satellite magnetometers?" *Tectonophysics*, vol. 431, nos. 1–4, pp. 173–195, Feb. 2007.

[39] E. Ghamry, A. G. Hafez, K. Yumoto, and H. Yayama, "Effect of SC on frequency content of geomagnetic data using DWT application: SC automatic detection," *Earth, Planets Space*, vol. 65, no. 9, pp. 1007–1015, Sep. 2013.

[40] A. G. Hafez and E. Ghamry, "Geomagnetic sudden commencement automatic detection via MODWT," *IEEE Trans. Geosci. Remote Sens.*, vol. 51, no. 3, pp. 1547–1554, Mar. 2013.

[41] A. G. Hafez, E. Ghamry, H. Yayama, and K. Yumoto, "A wavelet spectral analysis technique for automatic detection of geomagnetic sudden commencements," *IEEE Trans. Geosci. Remote Sens.*, vol. 50, no. 11, pp. 4503–4512, Nov. 2012.

[42] A. G. Hafez, E. Ghamry, H. Yayama, and K. Yumoto, "Systematic examination of the geomagnetic storm sudden commencement using multi resolution analysis," *Adv. Space Res.*, vol. 51, no. 1, pp. 39–49, Jan. 2013.

[43] E. Ghamry and A. Fathy, "A new method to calculate the time delay of the Pi2 pulsations," *Adv. Space Res.*, vol. 57, no. 2, pp. 701–709, 2016.

[44] M. Akhoondzadeh, A. De Santis, D. Marchetti, A. Piscini, and G. Cianchini, "Multi precursors analysis associated with the powerful Ecuador (MW = 7.8) earthquake of 16 April 2016 using Swarm satellites data in conjunction with other multi-platform satellite and ground data," *Adv. Space Res.*, vol. 61, no. 1, pp. 248–263, 2018.

[45] Z. Wan, Y. Zhang, Q. Zhang, and Z.-L. Li, "Validation of the land-surface temperature products retrieved from Terra moderate resolution imaging spectroradiometer data," *Remote Sens. Environ.*, vol. 83, nos. 1–2, pp. 163–180, Nov. 2002.

[46] Z. Wan, "New refinements and validation of the MODIS land-surface temperature/emissivity products," *Remote Sens. Environ.*, vol. 112, no. 1, pp. 59–74, Jan. 2008.

[47] Z. Wan, "New refinements and validation of the collection-6 MODIS land-surface temperature/emissivity product," *Remote Sens. Environ.*, vol. 140, pp. 36–45, Jan. 2014.

[48] D. Marchetti, A. De Santis, X. Shen, S. A. Campuzano, L. Perrone, A. Piscini, R. Di Giovambattista, S. Jin, A. Ippolito, G. Cianchini, C. Cesaroni, D. Sabbagh, L. Spogli, Z. Zhima, and J. Huang, "Possible lithosphere-atmosphere-ionosphere coupling effects prior to the 2018 Mw = 7.5 Indonesia earthquake from seismic, atmospheric and ionospheric data," *J. Asian Earth Sci.*, vol. 188, Feb. 2020, Art. no. 104097. [Online]. Available: http://www.sciencedirect.com/science/article/pii/S1367912019304493

[49] Z. Wan and J. Dozier, "A generalized split-window algorithm for retrieving land-surface temperature from space," *IEEE Trans. Geosci. Remote Sens.*, vol. 34, no. 4, pp. 892–905, Jul. 1996.

[50] *NASA Ocean Color*. Accessed: Oct. 21, 2020. [Online]. Available: https://oceancolor.gsfc.nasa.gov/

[51] R. Gelaro *et al.*, "The modern-era retrospective analysis for research and applications, version 2 (MERRA-2)," *J. Climate*, vol. 30, no. 14, pp. 5419–5454, Jul. 2017.

[52] W. Plastino, F. Bella, P. Catalano, and R. D. Giovambattista, "Radon groundwater anomalies related to the Umbria-Marche, September 26, 1997, earthquakes," *Geofisica Internacional*, vol. 41, no. 4, pp. 369–375, 2012.

[53] F. Vizzini and M. Brai, "In-soil radon anomalies as precursors of earthquakes: A case study in the SE slope of Mt. Etna in a period of quite stable weather conditions," *J. Environ. Radioactivity*, vol. 113, pp. 131–141, Nov. 2012.

[54] I. P. Dobrovolsky, S. I. Zubkov, and V. I. Miachkin, "Estimation of the size of earthquake preparation zones," *Pure Appl. Geophysics PAGEOPH*, vol. 117, no. 5, pp. 1025–1044, 1979.

[55] C. C. Finlay, N. Olsen, S. Kotsiaros, N. Gillet, and L. Tøffner-Clausen, "Recent geomagnetic secular variation from swarm and ground observatories as estimated in the CHAOS-6 geomagnetic field model," *Earth, Planets Space*, vol. 68, no. 1, p. 112, Dec. 2016.

[56] A. De Santis, G. Balasis, F. J. Pavón-Carrasco, G. Cianchini, and M. Mandea, "Potential earthquake precursory pattern from space: The 2015 nepal event as seen by magnetic swarm satellites," *Earth Planet. Sci. Lett.*, vol. 461, pp. 119–126, Mar. 2017.

[57] A. De Santis *et al.*, "Precursory worldwide signatures of earthquake occurrences on swarm satellite data," *Sci. Rep.*, vol. 9, no. 1, pp. 1–13, Dec. 2019.

[58] L. A. Zadeh, "Theory of filtering," *J. Soc. Ind. Appl. Math.*, vol. 1, no. 1, pp. 35–51, 1953.

[59] W. T. Cochran, J. W. Cooley, D. L. Favin, H. D. Helms, R. A. Kaenel, W. W. Lang, G. C. Maling, D. E. Nelson, C. M. Rader, and P. D. Welch, "What is the fast Fourier transform?" *Proc. IEEE*, vol. 55, no. 10, pp. 1664–1674, Oct. 1967.
[60] N. Ahmed, T. Natarajan, and K. R. Rao, "Discrete cosine transform," *IEEE Trans. Comput.*, vol. C-100, no. 1, pp. 90–93, Jan. 1974.
[61] C. C. Walton, W. G. Pichel, J. F. Sapper, and D. A. May, "The development and operational application of nonlinear algorithms for the measurement of sea surface temperatures with the NOAA polar-orbiting environmental satellites," *J. Geophys. Res. Oceans*, vol. 103, no. C12, pp. 27999–28012, Nov. 1998.

ESSAM GHAMRY was a Postdoctoral Associate with Kyung Hee University, South Korea, from 2014 to 2015, and Kyushu University, Japan, in 2020. He is currently a Research Professor with the National Research Institute of Astronomy and Geophysics, Cairo, Egypt. His current research interests include space geophysics, integrated studies of geomagnetic/geoelectric fields and space weather data using ground-based observatories and satellites inside the Earth's magnetosphere and ionosphere, earthquake precursor using ground/ionospheric data, and lithospheric magnetic field model using ground/space data.

EMAD K. MOHAMED received the B.Sc. degree in special geology and the M.Sc. degree in seismology from Al-Azhar University, in 2003 and 2011, respectively, and the Ph.D. degree in geophysics, seismology from Ain Shams University, Cairo, Egypt, in 2016. From 2013 to 2014, he joined the Ph.D. program as a regular student for One-year Ph.D. Courses with the Universidad Católica del Norte (UCN), Antofagasta, Chile. He is currently an Assistant Professor with the Department of Seismology, National Research Institute of Astronomy and Geophysics, Cairo. His research interests include seismotectonics, applications of near-surface geophysics, engineering seismology, and earthquake precursors using space data.

MOHAMED S. ABDALZAHER (Member, IEEE) received the B.Sc. degree (Hons.) in electronics and communications engineering, in 2008, the M.Sc. degree in electronics and communications engineering from Ain Shams University, Cairo, Egypt, in 2012, and the Ph.D. degree from the Electronics and Communications Engineering Department, Egypt-Japan University of Science and Technology, Madinet Borg Al Arab, Egypt, in 2016.

From 2015 to 2016, he was a Special Research Student with Kyushu University, Fukuoka, Japan. From April 2019 to October 2019, he was with the Center for Japan-Egypt Cooperation in Science and Technology, Kyushu University, where he was a Postdoctoral Researcher. He is currently an Assistant Professor with the National Research Institute of Astronomy and Geophysics, Cairo. His research interests include earthquake engineering, data communication networks, wireless communications, WSNs security, the IoT, and deep learning.

Dr. Abdalzaher was a TPC Member with the Vehicular Technology Conference and is a TPC Member with the International Japan-Africa Conference on Electronics, Communications and Computers. He is a Reviewer of the IEEE Internet of Things Journal, the IEEE Systems Journal, IEEE Access, *Transactions on Emerging Telecommunications Technologies*, *Applied Soft Computing*, the *Journal of Ambient Intelligence and Humanized Computing*, and *IET Journals*.

MOHAMED ELWEKEIL received the B.Sc. degree in electronics and electrical communications engineering from the Faculty of Electronic Engineering, Menoufia University, Egypt, in 2007, and the M.Sc. and Ph.D. degrees in electronics and communications engineering from the Egypt-Japan University of Science and Technology (E-JUST), Alexandria, Egypt, in 2013 and 2016, respectively. From December 2007 to November 2016, he was a Teaching Assistant with the Department of Electronics and Electrical Communications Engineering, Faculty of Electronic Engineering, Menoufia University, Egypt. He has been promoted to a Lecturer (Assistant Professor) position with the Department of Electronics and Electrical Communications Engineering, in December 2016. From April 2014 to March 2015, he was a Research Intern with Alcatel-Lucent Bell N.V. (now NOKIA), Antwerp, Belgium, where he was working on WiFi optimization project. He joined Kyushu University, Fukuoka, Japan, as a Special Research Student, in October 2015, for a period of nine months. From April 2018 to March 2020, he was with the College of Information Engineering, Shenzhen University, Shenzhen, China, where he was working as a Postdoctoral Researcher. His research interests include radio resource management for wireless networks, spatial modulation, signal processing for communications, and earthquakes engineering.

DEDALO MARCHETTI received the degree in astronomy and astrophysics and the Ph.D. degree in physics with a thesis about measurement of polarization of exoplanets. Since 2016, he has been working with the Italian National Institute of Geophysics and Volcanology. Since 2018, he has been working with NUIST University. His current research interests include analyse the variations of the Earth's magnetic field to search for possible precursors of earthquakes by satellite and ground measurements. He is also developing statistical and case studies analysis for research for other earthquake effects in atmosphere and ionosphere.

ANGELO DE SANTIS is currently the Director of Research with INGV and former Professor of Geophysics with the University of Chieti-Pescara and Professor of Geomagnetism and Applied Geophysics at the Ph.D. courses of Rome La Sapienza and Roma Tre Universities. He was the Coordinator of ESA funded project SAFE, and is responsible for seismo-associated phenomena study in the present ASI funded project Limadou-science. He is also present scientific responsible of the Italian Government (MIUR) funded project InSea. His main research interest includes understanding how the planet works, and its layers interact, with particular attention to mechanic and electromagnetic couplings, so including the studies under the disciplines of geosystemics, seismotectonics, geomagnetism, and ionospheric physics.

MOSTAFA HEGY received the M.Sc. degree in geophysics from Minufiya University, Egypt, in 2018. He currently works as a Researcher Assistant with the National Research Institute of Astronomy and Geophysics. His research interests include space geophysics using magnetic field data form swarm satellites and space weather studies and land magnetic surveys using magnetotelluric, proton and over hauser magnetometers.

AKIMASA YOSHIKAWA is currently a Professor of geophysics with the Department of Earth and Planetary Sciences, Faculty of Science, Kyushu University, Japan, where he is also with the International Center for Space Weather Science and Education. He is the PI of MAGDAS network. His main research interests include magnetosphere-ionosphere coupling, substorm, simulation, and mathematical science.

ADEL FATHY received the Ph.D. degree in geomagnetism from the Physics Department, Faculty of Science, Fayoum University, Egypt. He is currently a Lecturer with the Physics Department, Faculty of Science, Fayoum University. His research interests include space science (magnetospheric-ionospheric interactions), study the state of the magnetosphere and the ionosphere and investigates space phenomenon affect the propagation of electromagnetic signals, such as GPS and trans-ionospheric signals, and modeling the Earth's magnetic field and its secular variations using satellite data.